Non-locality of the contact line in dynamic wetting phenomena.

Alex V. Lukyanov

School of Mathematical and Physical Sciences, University of Reading, Reading RG6 6AX, UK

E-mail: a.lukyanov@reading.ac.uk

Abstract

In a large category of wetting phenomena, the contact line was always regarded as a compact, one-dimensional object with only microscopic length scales involved. This prevailing opinion had a certain impact and repercussions on the developing theories, interpretation of experimental results and the subsequent modeling methodologies. In this report, we will demonstrate, on the basis of rst principles of molecular dynamic simulations, that this is not always the case. In particular, this is not true in the complete wetting case, when the advancing contact line motion is often accompanied by a running ahead precursor lm. We study the onset of the dynamic wetting regime with the precursor lm present and its main characteristic properties, such as dimensions. We show how the contact line becomes wide and practically macroscopic, and how the presence of the precursor lmprinciple captured by a localized approach.

Keywords: wetting, nano-scale, meso-scale, contact line, molecular dynamics simulations.

Introduction

In 1805, Thomas Young proposed an equation to predict the value of the equil.u96yn31so-sion28(ntact)] asle of a ieque,f

line. In equilibrium, at zero contact line velocity, the friction force $F = 0$ vanishes and the contact angle should attain the equilibrium value $_0$ in the absence of the hysteresis e ects.

In both static and dynamic scenarios recreated in molecular dynamics simulations (MDS), the local character of the contact line was directly established. It was found that the contact line region, including the domain where the contact line friction force F was generated, was on the microscopic length scale of a few or so atomic distances, that is basically around one or two nanometers in dimensional units.[7,8] In fact, the analysis and simulations performed in[8] have con rmed the longstanding hypothesis postulated in the molecular kinetic theory[9,10] about the existence of a friction force of non-hydrodynamic, that is of microscopic origin acting directly on the contact line and leading to the modi ed Young's law (2).

As one can see, the locality of the contact line region has important repercussions for the modelling of the dynamic wetting phenomena. In the current study, we consider a situation, when the local character of the contact line region is completely broken.

In general, non-locality in dynamic wetting is often associated with the presence of surface tension gradients (Marangoni e ect) created by gradients of temperature or relative concentrations of surface phase components.[11] In this case, hydrodynamic motion can in uence surface tension gradients on macroscopic length scales and therefore a ect the local contact angle. The contact angle can be in uenced directly if the system size is on the length scale comparable to the size of the contact line region, basically in the nano ow conditions.[12] In simple liquids at constant temperature, the interfaces areb in)-amitn)-amrium

To mimic the forced wetting regime, the solid wall particles were moving with velocity U in the z-direction ([1,0,0] crystallographic direction), where the re ective wall was acting as a piston at rest. After initial equilibration during $t_{eq} = 10000\ _0$ with the time integration step $t_s = 0{:}01\ s$

Figure 1: Snapshots of the cylindrical droplets in a steady state in MDS set-up at H 57 and two dynamic contact angles: $_c$ = 122:7 1 at U = 0:06 u_0 and $_c$ = 68:7 1 at U = 0:009 u_0. The set-up is periodic in the x-direction with the total number of liquid particles in the simulations varied between 90; 000 to 140; 000. The solid wall was moving along the z-direction aligned in the [1,0,0] crystallographic direction of the fcc lattice comprising the solid substrate. The steady state was reached following an equilibration period of 10000 $_0$.

agates according to the di usion law,

$$L_p = \sqrt{D_s t} \qquad (3)$$

similar to the well-known in the capillary science Lucas-Washburn propagation dynamics. Here L_p is the length of the precursor lm counted from the foot of the macroscopic liquid region and D_s is e ective coe cient of surface di usion. As one can readily observe, the velocity of the moving lm front

$$\frac{dz_f}{dt} = \frac{1}{2}\sqrt{\frac{D_s}{t}} = \frac{D_s}{2L_p} \qquad (4)$$

vanishes with time as the lm length increases. This in turn implies that in a moving contact line problem, when, for example, a droplet is moving with macroscopic velocity U and the tip of the precursor lm is propagating independently at the rate dz_f/dt in the same direction, the length of the precursor lm is expected to attain a constant value de ned by the droplet velocity and the coe cient of the surface di usion

$$L_p = \frac{D_s}{2U} \qquad (5)$$

when

$$\frac{dz_f}{dt} \quad U = \frac{dL_p}{dt} = 0: \qquad (6)$$

In our MDS, the precursor lm is only observed in the complete wetting cases ($_0 = 0$), when the droplet velocity is below some critical value $U < U_T$, Tables 1 and 2. The steady state of the precursor lm is indeed observed and is illustrated in Fig. 2. As one can see from the averaged density pro les at the foot of the wetting volume, the thickness of the lm is about one atomic diameter . This is the typical morphology of the precursor lms observed in our MDS in the liquids consisting of both short chain ($N_B = 5$) and long chain ($N_B = 50$) molecules. Consider now the obtained steady state in detail.

Results and discussion

Consider rst how do our MDS results correspond to the predictions of the di usion theory represented by equation (3).

Figure 3: Illustration of the precursor lm dynamics while the system was reaching the steady state in MDS set-up. Precursor lm length L_p as a function of time t at di erent contact line velocities U and molecular length N_B at $T = 1"$ $=k_B$. The solid lines are the t given by equation (8).

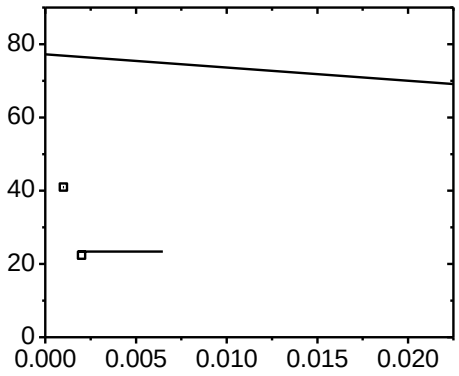

Figure 4: Precursor lm length L_p as a function of the droplet velocity U in a steady state at di erent system parameters T, N_B and $"_{wf}$. The solid lines are the t $L_p = D_s/2U$.

Evolution of the precursor lm

Integrating the evolution equation

$$\frac{dL_p}{dt} = \frac{D_s}{2L_p} \quad U \qquad (7)$$

Table 1: Parameters of the MDS systems and dynamic wetting regimes: N_B

of the lm. Note, in the tting procedure, only one parameter D_s in (8) has been allowed to vary.

with characteristic dimensions $z = 1$ and $y = 3$, and by averaging over the time interval $t = 10000\ _0$ and over the droplet depth in the x-direction. The distribution as a function of the tangential coordinate z has two characteristic regions, Fig. 6 (a). The first part of the distribution has a characteristic bell-shaped form and begins at the tip of the density distribution at the substrate. Further along the substrate, the bell-shaped region goes into a tail. We note that the characteristic length scale of the friction force variations is definitely microscopic.

The tail of the friction force distribution in our simulations is due to the small, finite size of the system H and corresponds well to the shear stress developed in the rectilinear flow between the solid substrates. Indeed, in the example shown in Fig. 6 (a), the shear stress in the tail region at $z > 20$ at the solid substrate was found to be $_{yz} = 0{:}082 \quad 0{:}006\, f_0$, while the value of $_{yz} = \frac{6\ U}{H_e} = 0{:}073\, f_0$ is expected assuming the Hagen-Poiseuille flow between the planes, where $H_e = H \quad 2\ _S$ 52 is the effective gap between the plates taking into account the size of the solid substrate $_S \quad 2{:}75$.

As the system size increases, the value of the friction force in the tail region is observed to decrease at a given substrate velocity, as is expected in the rectilinear Hagen-Poiseuille flow conditions, and to eventually disappear in the macroscopic limit $H \ ! \ 1$.[8] At the same time, the bell-shaped region in this limiting procedure is shown to be qualitatively invariant (subject

changes, though the concept itself is still useful. In a nutshell, the usually microscopic object, the contact line becomes geometrically macroscopic due to the developing precursor lm. As a result, the processes usually taking place on the scale of a nanometer, are now occurring over much larger, tens of nanometers length scales. In terms of the macroscopic observables, the contact angle velocity dependence attains a

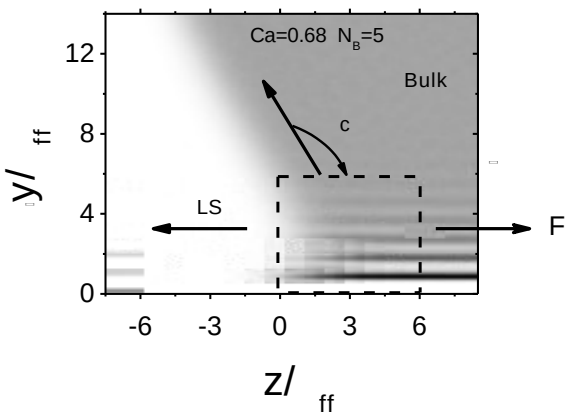

Figure 7: MDS in the complete wetting case, set (c) in Table 1, at the substrate velocity $U = 0{:}06\,u_0$ and the dynamic contact angle $_c = 123$. Force balance and the density distribution at the contact line region. The dashed box designates the contact line region. Distance y is measured from the equimolar surface of the solid wall particles, while distance z is measured from the centre of the simulation box.

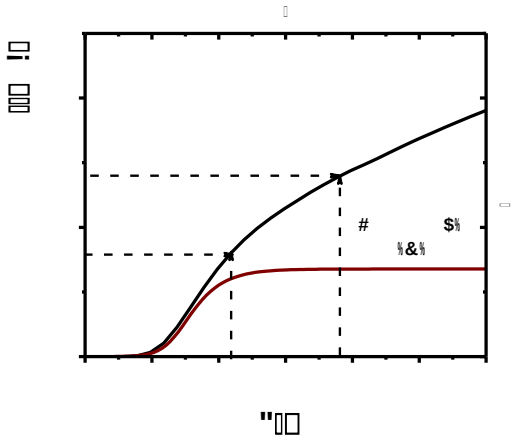

Figure 8: MDS in the complete wetting case, set (c) in Table 1, at the substrate velocity $U = 0{:}06\,u_0$ and the dynamic contact angle $_c = 123$. The upper solid line (black) is for the integrated friction force $F_D = \int_{z_0}^{R_z} F\,d$ as a function of z at $z_0 = 5$. The second, lower solid line (brown) is the integrated force in the macroscopic limit at the same system parameters. The dashed lines designate the contact line region as the interface crossover shown in Fig. 7 by the dashed box and the integration region to achieve the force balance $F_D + _{LS} + \cos _c = 0$.

Figure 9: MDS in the complete wetting case, set (c) in Table 1, at the substrate velocity $U = 0{:}06\,u_0$ and the dynamic contact angle $_c = 123$. The force F_S per unit length (in the x-direction) acting on the surface of the variable side size y oriented perpendicularly to the z-axis and located at the right end of the dashed box in Fig. 7. The dashed line is the linear t $F_S = A + B(y - y_0)$ at $A = 2{:}3 \quad 0{:}1 \;_0$, $y_0 = 0{:}44 \quad 0{:}1$ and $B = 0{:}78 \quad 0{:}02 f_0$.

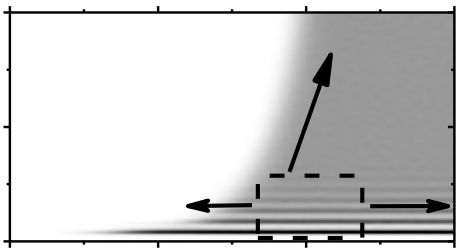

Figure 10: MDS in the complete wetting case, set (c) in Table 1, at the substrate velocity $U = 0{:}009\,u_0$ and the dynamic contact angle $_c = 68{:}7$. Force balance and the density distribution at the contact line region. The dashed box designates the contact line region. Distance y is measured from the equimolar surface of the solid wall particles, while distance z is measured from the centre of the simulation box.

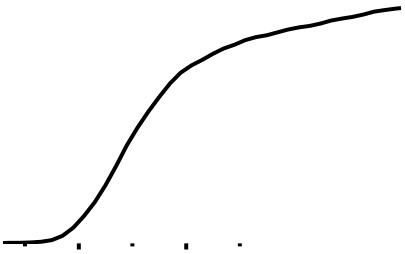

Figure 12: MDS in the complete wetting case, set (c) in Table 1, at the substrate velocity $U = 0{:}009\, u_0$ and the dynamic contact angle $_c = 68{:}7$. The integral of the tangential component of the friction force $\int_{z_0}^{z} F\, d$ as a function of z.

that m_f , , " and $_0 =$ $\sqrt{\frac{m_f}{"}}$ provide basic scales for mass, length, energy and time respectively. At the same time, ^{3}, $u_0 =$ $" m_f {}^{1}$, $f_0 = " {}^{3}$, $_0 = " {}^{2}$ and $_0 =$ $p\overline{" m_f {}^{2}}$ provide necessary scales for particle density, velocity, pressure,0 13.186 6.939 Td [(p)]TJ ET q 1 0 t72

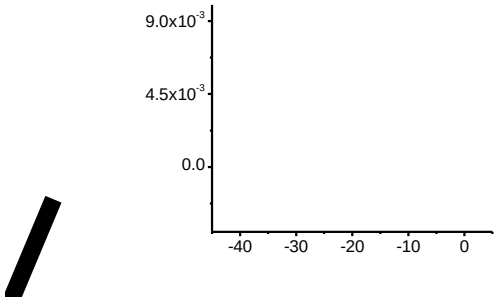

Figure 11: MDS in the complete wetting case, set (c) in Table 1, at the substrate velocity $U = 0{:}009\, u_0$ and the dynamic contact angle $_c = 68{:}7$. (a) Tangential component of the friction force F , (b) surface density $_S$ and (c) surface velocity v_S as functions of z. The dashed box designates the contact line region, with similar dimensions as in Fig. 7. The surface variables have been obtained in the boundary layer $y = 1{:}5$ at the solid wall.

means of harmonic potential $_a = x^2$, with the strength $= 800 \frac{"}{^2}$ chosen such that the root-mean-square displacement of the wall atoms $p\overline{< r^2 >}$ was small enough to satisfy the Lindemann criterion for melting $p\overline{< r^2 >} < 0{:}15\ _{ww}$. The strength of the harmonic potential was su cient to guarantee rigidity of the solid wall, so that elasto-capillarity e ects can be neglected, that is $(=)^{1=2}$ 1, where is equilibrium liquid-gas surface tension.[23] The anchor points in the layer of the solid wall facing the liquid molecules have been slightly randomized in the vertical y direction, with the amplitude $p\overline{< y^2 >} = 0{:}3$. This small roughness allowed to avoid undesirably large slip lengths observed in MDS[21] and any bias towards ideal substrates in this study. The substrate density $_S$ was set to $_S = 1{:}41\ ^3$ with the liquid-solid interaction length scale $_{wf} =$ and the solid-solid interaction length scale $_{ww} =$. Two parameters of the model, temperature T and strength of the liquid-solid interactions $"_{wf}$ have been varied in the simulations to obtain liquids with di erent viscosities and to emulate various wetting conditions (partial, $_0 > 0$, or full wetting, $_0$

in the case of a free surface, and by

$$_{LS} = \int_0^{L_y} \left(\frac{_{zz} + _{xx}}{2} - _{yy} \right) y \, (y) \frac{d \, _S}{dy} \, dy \qquad (14)$$

for a solid-liquid interface, where $_S$ is the potential of the solid wall forces acting on the liquid particles and is the particle density.[25,26] The liquid-solid surface tension is calculated in the assumption of undeformable solid substrate, so that $_{LS}$ is in fact the surface tension of the liquid.

The value of the zero shear rate viscosity in the liquid in the bulk conditions is evaluated by considering the correlation function

$$= \frac{V}{k_B T} \int_0^{1} < \quad (t) \quad (0) > dt$$

at ~~6~~ , details can be found in.[27]

The methodology of the surface tension evaluation in MDS has been veri ed either by comparison with the Laplace law (by independently evaluating surface tension and the pressure in a large, levitating liquid drop)[28] or by comparison with the Young-Dupre equation in equilibrium $\cos _0 = _{LS} + _{GS}$.[29] The Young-Dupre equation was probed by evaluating independently surface tensions and by directly measuring the equilibrium contact angle $_0$ from the shape of the free-surface pro les of cylindrical droplets.[29,30] The di erence between two static contact angles (measured geometrically and calculated via the Young-Dupre equation) was found not to exceed the accuracy of the contact angle evaluations.

Evaluation of the contact angles in MDS

The contact angle in our study has been inferred from the free-surface pro les de ned as the locus of equimolar points and averaged over the x-direction, Fig. 1 and during the time period of $t = 10000 \, _0$. The pro les were developed by means of a circular t

$$(y \quad y_0)$$

has been applied to a part of the free-surface pro le of length 20 excluding h_s layer adjacent to the substrate corresponding to the liquid-solid interface, similar to the methodology developed in.[30] The accuracy of this approach is illustrated in Figs. 14 and 15. One may notice that the interface shape is very well described by the t even at Ca > 1. The value of the cut-o distance h_s was varied in between 4 h_s 8 to exclude the area strongly a ected by the solid wall potential with density variations on the scale of one atomic distance .

Figure 15: Illustration of the free surface pro-les (equimolar surfaces approximated by the t (15), shown by the dashed line) developed from the particle density distributions obtained in MDS in a steady state in the case of complete wetting $_0$ = 0 at N_B = 50, T_0 = 1" =k_B and "$_{wf}$ = 1:3" . Here, (a) $_c$ = 90 1 , U = 0:01 u_0, Ca = 0:67 and (b) $_c$ = 128:3 1 , U = 0:1 u_0, Ca = 6:7. In both cases h_s = 8 and the distance y is measured from the equimolar surface of the substrate particles of the bottom plate, while the distance z is calculated from the centre of the simulation box, as in Fig. 1.

References

(1) Young, T. An essay on the cohesion of u-ids Phil. Trans. R. Soc. London 1805, 95, 65{87

(2) Leger, L. and Joanny, J.F. Liquid spreading Rep. Prog. Phys. 1992, 55, 431{486

(3) Roura, P. and Fort, J. Local thermodynamic derivation of Young's equation J. Colloid Interface Sci. 2004, 272, 420{429

(4) Finn, R. The contact angle in capillarity Phys. Fluids 2006, 18, 047102

(5) Ingebrigtsen, T. and Toxvaerd, S. Contact Angles of Lennard-Jones Liquids and Droplets on Planar Surfaces J. Phys. Chem. C 2007, 111, 8518{8523

(6) Snoeijer, J.H. and Andreotti, B. A microscopic view on contact angle selection Phys. Fluids 2008, 20, 057101

(7) Seveno, D.; Blake, T.D. and De Coninck, J. Young's Equation at the Nanoscale Phys. Rev. Lett. 2013, 111, 096101

(8) Lukyanov, A.V. and Likhtman, A.E. Dynamic Contact Angle at the Nanoscale: A Uni ed View ACS Nano 2016, 10, 6045{6053

(9) Blake, T.D. and Haynes, J.M. Kinetics of Liquid/Liquid Displacement. J. Colloid Interface Sci. 1969, 30, 421{423

(10) Blake, T.D. The physics of moving wetting lines J. Colloid Interface Sci. 2006, 299, 1{13

(11) Darhuber, A.A. and Troian, S.M. Principles of micro uidic actuation by modulation of surface stresses Annu. Rev. Fluid Mech. 2005, 37, 425{455

(12) Blake, T.D.; Fernandez-Toledano, J.C.; Doyen, G. and De Coninck, J. Forced wetting and hydrodynamic assist Phys. Fluids 2015, 27, 112101

(13) Heslot, F.; Fraysse, N. and Cazabat, A.M. Molecular layering in the spreading of wetting liquid drops Nature 338, 640{642 1989,

(14) Heslot, F.; Cazabat, A.M. and Fraysse, N. Di usion-controlled wetting lms J. Phys. Condens. Matter 1, 5793{5798 1989,

(15) Cazabat, A.M.; Fraysse, N.; Heslot, F. and Carles, P. Spreading at the Microscopic Scale J. Phys. Chem. 94, 7581{7585 1990,

(16) Cazabat, A.M.; Fraysse, N.; Heslot, F.; Levinson, P.; Marsh, J.; Tiberg, F. and Valignat, M.P. Pancakes Adv. Colloid Interface Sci. 48, 1{17 1994,

(17) Ala-Nissila, T.; Herminghaus, S.; Hjelt, T. and Leiderer, P. Di usive Spreading of Chainlike Molecules on Surfaces Phys. Rev. Lett. 76, 4003{4006 1996,

(18) Chibbaro, S.; Biferale, L.; Diotallevi, F.; Succi, S.; Binder, K.; Dimitrov, D.; Milchev, A.; Girardo, S. and Pisignano, D. Evidence of thin- lm precursors formation in hydrokinetic and atomistic simulations of nano-channel capillary lling EPL 84, 44003 2008,

(19) Popescu, M.N.; Oshanin, G.; Dietrich, S. and Cazabat, A.M. Precursor lms in wetting phenomena J. Phys. Cond. Matter 24, 243102 2012,

(20) Thompson, P.A.; Troian, S.M. A general boundary condition for liquid ow at solid surfaces Nature 1997, 389, 360{362

(21) Priezjev, N.V. Relationship Between Induced Fluid Structure and Boundary Slip in Nanoscale Polymer Films. Phys. Rev. E 2010, 82, 051603

(22) Kremer, K.; Grest, G.S. Dynamics of Entangled Linear Polymer Melts: A Molecular-Dynamics Simulation. J. Chem. Phys. 92, 5057{5086 1990,

(23) Weijs, J.H.; Andreotti, B.; Snoeijer, J.H. Elasto-Capillarity at the Nanoscale: on the Coupling Between Elasticity and Surface Energy in Soft Solids. Soft Matter 2013, 9, 8494{8503

(24) Irving, J.H., Kirkwood, J.G. The Statistical Mechanical Theory of Transport Processes. IV. The Equations of Hydrodynamics J. Chem. Phys. 1950, 18, 817{829

(25) Scho eld, P., Henderson, J.R. Statistical Mechanics of Inhomogeneous Fluids P. Roy. Soc. A-Math. Phy. 1982, 379, 231{246

(26) Navascues, G. Liquid surfaces: theory of surface tension. Rep. Prog. Phys. 1979, 42, 1131{1186

(27) Likhtman, A.E.; Sukumaran, S.K.; Ramirez, J. Linear Viscoelasticity from Molecular Dynamics Simulation of Entangled polymers. Macromolecules 2007, 40, 6748{6757

(28) Lukyanov, A.V.; Likhtman, A.E. Relaxation of Surface Tension in the Free-Surface Boundary Layer of Simple Lennard-Jones Liquids. J. Chem. Phys. 2013, 138, 034712

(29) Lukyanov, A.V.; Likhtman, A.E. Relaxation of Surface Tension in the Liquid-Solid Interfaces of Lennard-Jones Liquids. Langmuir 2013, 29, 13996{14000

(30) Lukyanov, A.V.; Pryer, T. Hydrodynamics of moving contact lines: Macroscopic versus microscopic. Langmuir 2017, 33, 8582{8590